Hemp-derived Activated Carbon Supported Zero-valent Iron as a Heterogeneous Fenton Catalyst for the Treatment of Pulping Effluent

Lihuan Mo, Sizai Zhou, Shuang Yang, Jie Gong, and Jun Li *

Hemp fiber was applied to prepare activated carbon by phosphoric acid activation at a carbonization temperature of 400 °C. Then, zero-valent iron particles were immobilized onto the surface of hemp-derived AC (HAC), and the composites (ZVI@HAC) were used as heterogeneous catalysts for Fenton-like treatment of pulping effluent. The as-prepared catalysts were characterized. The optimum conditions for Fenton-like reaction and the reusability of the catalyst were investigated. Results showed that ZVI particles were well-distributed on the surface of HAC without aggregation. Both HAC and ZVI@HAC had a microporous structure. With the loading of ZVI, the catalysts were endowed with magnetism and more active sites. Under the optimal conditions (3.0 initial pH, 35 mmol/L H_2O_2, and 3.0 g/L 2-ZVI@HAC), the chemical oxygen demand (COD) removal rate reached 87.74%. This work illustrated the feasibility of HAC as a carrier of ZVI and the ZVI@HAC was an effective heterogeneous Fenton catalyst.

Keywords: Hemp fiber; Activated carbon; Zero-valent iron; Fenton-like oxidation; Pulping effluent

*Contact information: State Key Laboratory of Pulp and Paper Engineering, South China University of Technology, Guangzhou, 510640 China; *Corresponding author: ppjunli@scut.edu.cn*

INTRODUCTION

Effluents of pulp and paper industry are highly polluted by various types of recalcitrant organic compounds, such as phenolic compounds, saccharides, and carboxylic acids (He *et al.* 2018). These pollutants are either formed during lignin decomposition or introduced by adding needed chemicals during pulping and papermaking processes (Kamali and Khodaparast 2015). Conventional physical-chemical and biological treatments are not effective for the complete degradation of these recalcitrant organic pollutants (Krishna *et al.* 2014).

Due to strong decontamination ability against organic contaminants, advanced oxidation processes (AOPs), such as the Fenton reaction, have received more attention in recent years (Merayo *et al.* 2013). In a traditional Fe^{2+}/H_2O_2 Fenton system, the soluble Fe^{2+} catalyzes the hydrogen peroxide reaction to produce hydroxyl radicals with strong oxidation ability (Neyens and Baeyens 2003). However, the production of metal sludge, a narrow pH range, and slow transformation rate of the Fe^{3+}/Fe^{2+} redox couple limit its practical application (Bello *et al.* 2019). In pursuit of overcoming these limitations, heterogeneous Fenton catalysis has been developed from the classic Fenton process (Arimi 2017). In the heterogeneous Fenton process, solid iron catalysts have the capability to generate hydroxyl radicals from hydrogen peroxide in a wide range of pHs and prevent the generation of iron sludge (Rubeena *et al.* 2018).

Zero-valent iron (ZVI) has been investigated as a heterogeneous Fenton catalyst due to its high surface activity (Tosco *et al.* 2014). Compared with conventional iron

catalysts, the application of ZVI can give rise to Fe^{2+} generation in acidic solution, leading to rapid decomposition of hydrogen peroxide (Deng *et al.* 2018). Moreover, a continuous supply of Fe^{2+} is given due to the reaction between Fe^0 and Fe^{3+} generated from corrosion of the ZVI surface (Li *et al.* 2006).

Nevertheless, due to interparticle interactions, such as van der Waals forces and magnetic interactions (Bhaumik *et al.* 2015), ZVI particles generally tend to aggregate into large clusters, resulting in reduced reactivity and reusability. To lighten the aggregation of ZVI particles, a series of support materials have been used in combination with ZVI, such as ordered mesoporous carbon, attapulgite, graphene oxide, and biochar (Dai *et al.* 2016; Hussain *et al.* 2017; Zhang *et al.* 2019). Based on previous studies, a good carrier of ZVI should be inexpensive, environmentally friendly, and able to prevent agglomeration.

Activated carbon (AC) has become a common adsorbent material and catalyst carrier due to its large surface area and porosity (Vandarkuzhali *et al.* 2018). Most commercial ACs are produced from fossil fuel-based precursors, which make them expensive and environmentally unfriendly. Hence, ACs synthesized from agricultural waste have gained much attention. Investigation into the preparation of ACs from several agricultural byproducts, such as coffee endocarp (Nabais *et al.* 2008), porous beetroot (Veerakumar *et al.* 2016), coconut shells (Yang *et al.* 2010), and potato peels (Kyzas *et al.* 2016), has been reported.

Hemp grows quickly in most locations and climates, making it a valuable and environmentally friendly crop. Hemp has been used in many fields, such as the production of paper, medicine, ink, and fuel. It is also used in the production of carbon materials due to its different porous structure in the cross-section and longitudinal section (Liu *et al.* 2017). The application of hemp-derived activated carbon (HAC) in the field of adsorption has been studied. Rosas *et al.* (2008) reported that HAC was prepared for the adsorption of water vapor. Vukčević *et al.* (2015) found that activated carbon derived from waste hemp has great performance in pesticide adsorption. Carbon materials from waste short hemp fibers were prepared and used for adsorption of heavy metal ions (Vukčević *et al.* 2014). However, the performance of HAC as a catalyst carrier has been less explored.

The main aim of this research was to synthesis and characterize ZVI@HAC and its performance as a heterogeneous catalyzing H_2O_2 over Fenton-like treatment of pulping effluent. The removal rate of COD was evaluated as a function of operational factors like iron content, pH, H_2O_2 dosage, and catalyst loading. In the end, a possible catalytic mechanism is proposed.

EXPERIMENTAL

Materials and Chemicals

Phosphoric acid, iron acetylacetonate [$C_{15}H_{21}FeO_6$], mercuric sulfate, toluene, and ethanol were purchased from Macklin Chemical Reagent Co., Ltd. (Shanghai, China). Hydrogen peroxide, silver sulfate, potassium dichromate solution, and sodium hydroxide were purchased from Fuchen Chemical Reagent Co., Ltd. (Tianjin, China).

Original hemp stalk was collected from the Guangxi region of China. The effluent in this study was collected from a bagasse pulp mill in the Guangxi region of China, after biological treatment and before the following advanced treatment. The main properties of the effluent were: 278 mg/L chemical oxygen demand (COD), 62.2 mg/L total organic carbon (TOC), 260 Color Unit (C.U.) color, and pH 8.2.

Preparation of HAC and ZVI@HAC

A sample of 10 g hemp fiber and 250 mL H_3PO_4 solution (3 mol/L) were placed in a conical flask. The mixture was stirred in a water bath at 98 °C for 4 h. Activated hemp fibers were dried at 60 °C for 12 h. Then, the sample was heated to 200 °C in a nitrogen atmosphere at a rate of 5 °C/min and held at this temperature for 120 min to remove traces of water. Finally, the H_3PO_4-impregnated sample was heated at a rate of 5 °C/min up to 400 °C in a nitrogen atmosphere and kept at this temperature for 60 min. The sample (HAC) was cooled under constant N_2 flow, washed to neutral, and dried at 105 °C.

The ZVI@HAC was prepared *via* a solvothermal-carbonthermal method. A sample of 1.0 g HAC and a certain amount of iron acetylacetonate were dispersed in a mixture solution of 50 mL. After ultrasonic dispersion for 120 min, the above mixture was dried at 200 °C for 120 min and then calcined at various temperatures (600 °C, 700 °C, 800 °C, and 900 °C) for 3 h. After the optimal formation condition of ZVI were determined, all catalysts were synthesized at a fixed temperature. The relationship between the mass ratio of Fe/C and the catalyst name was shown in the Table 1.

Table 1. Name System of ZVI@HAC

Samples	Mass of Iron Acetylacetonate (g)	Mass of HAC (g)	Annealing Temperature (°C)
0.5-ZVI@HAC	0.5	1.0	800
1-ZVI@HAC	1.0	1.0	800
2-ZVI@HAC	2.0	1.0	800
3-ZVI@HAC	3.0	1.0	800
4-ZVI@HAC	4.0	1.0	800

Fenton-like Oxidation Method

All Fenton-like reactions were performed in a shaker incubator at a temperature of 25 °C. A sample of 200 mL pulping effluent and a specific amount of catalyst were first added to a 250 mL conical flask. Sulfuric acid was used to adjust the pH to desired values. Then, reactions were started by adding a certain amount of H_2O_2. At defined time intervals, proper solution samples were removed and put through a 0.45-μm water phase needle filter membrane to remove catalyst particles.

Characterization Methods

X-ray diffraction analysis

The crystalline phases of catalysts were determined using a Bruker D8 advance X-ray diffractometer (Bruker Corporation, Billerica, MA, USA) that employed CuKα radiation at 40 kV and 40 mA. Continuous scans from 2θ at 10° to 80° were collected at a scanning speed of 3°/min.

Raman spectroscopy analysis

Raman spectra were recorded on a spectrometer (LabRAM Aramis, Horiba, Ltd., Kyoto, Japan), which employed 532.0 nm wavelength laser light.

Brunauer-Emmett-Teller (BET) test

The BET surface area, pore volume, and pore size of catalysts were measured by N_2 adsorption-desorption technique at 77 K using a Micromeritics ASAP 2020 BET surface area analyzer (Micromeritics Instrument Corporation, Norcross, GA, USA).

Scanning electron microscopy (SEM)

Morphology of the samples was studied by scanning electron microscopy (MERLIN Compact, Carl Zeiss, Oberkochen, Germany). Images were recorded at different magnifications at an operating voltage of 5 kV. Elemental compositions of samples were analyzed with an energy dispersive spectroscopy (EDS) analyzer.

Magnetic properties

Magnetic properties of catalysts were characterized by a vibrating sample magnetometer (VSM) (Lake Shore Cryotronics, Westerville, OH, USA) at room temperature.

Chemical oxygen demand

The COD values were measured according to Standard Methods for the Examination of Water and Wastewater (ISO 6060-1989).

Ultraviolet (UV) spectroscopy analysis and Gas chromatography-mass (GC-MS) spectrometry analysis

The UV-visible (Vis) diffuse reflectance spectra of the effluent were obtained on an UV-Vis NIR spectrophotometer (UV-2600; Shimadzu Corporation, Kyoto, Japan) with a component of integrating spheres in the range of 190 nm to 900 nm. The investigation of the oxidation products was performed by Gas chromatography-mass spectrometry analysis (GC–MS, Agilent 7890A).

RESULTS AND DISCUSSION

Effect of Annealing Temperature on the Catalyst Structure

The annealing temperature had a great influence on the formation of zero-valent iron and its fixation on carbon materials. To show the crystallographic structures of the catalysts prepared at various temperatures, the powder XRD patterns of samples are shown in Fig. 1.

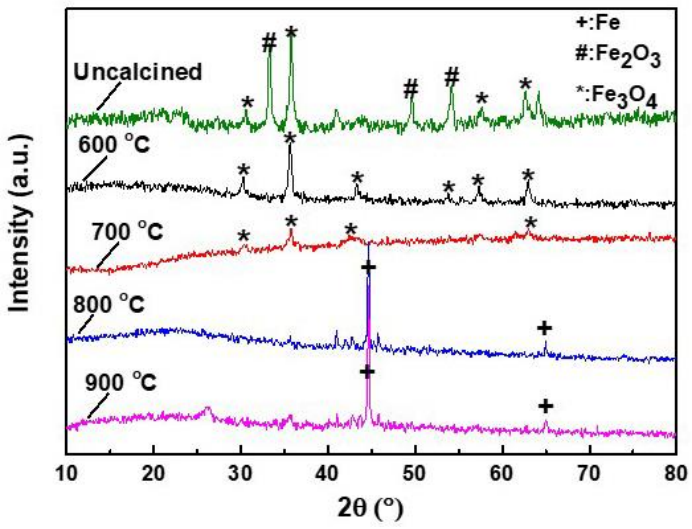

Fig. 1. XRD patterns of samples prepared at various temperatures

Characteristic peaks at 2θ = 33.2°, 49.5°, and 54.2° were observed in uncalcined samples due to the formation of Fe_2O_3 (Su *et al.* 2015). Two main broad diffractions at 2θ = 35.42° and 43.05° that existed in the catalysts prepared at 600 °C and 700 °C, respectively, could be attributed to planes of Fe_3O_4 (Yiu *et al.* 2010). Compared to the XRD patterns of the above samples, a new diffraction peak at 44.84° and a relatively smaller peak at 65.14° were shown in the XRD patterns of the catalysts prepared at 800 °C and 900 °C, respectively, which suggested that zero-valent iron particles were successfully loaded on HAC (Mortazavian *et al.* 2018). This was attributed to the formation of the zero-valent iron through the stated reaction of iron and carbon at high temperatures (Hoch *et al.* 2008).

Batch Experiments for Fenton-like Oxidation

The parameters, such as iron content, initial pH, H_2O_2 dosage, and catalyst loading, had great influence on the performance of Fenton-like reaction. To obtain the most suitable reaction conditions, a series of experiments was performed.

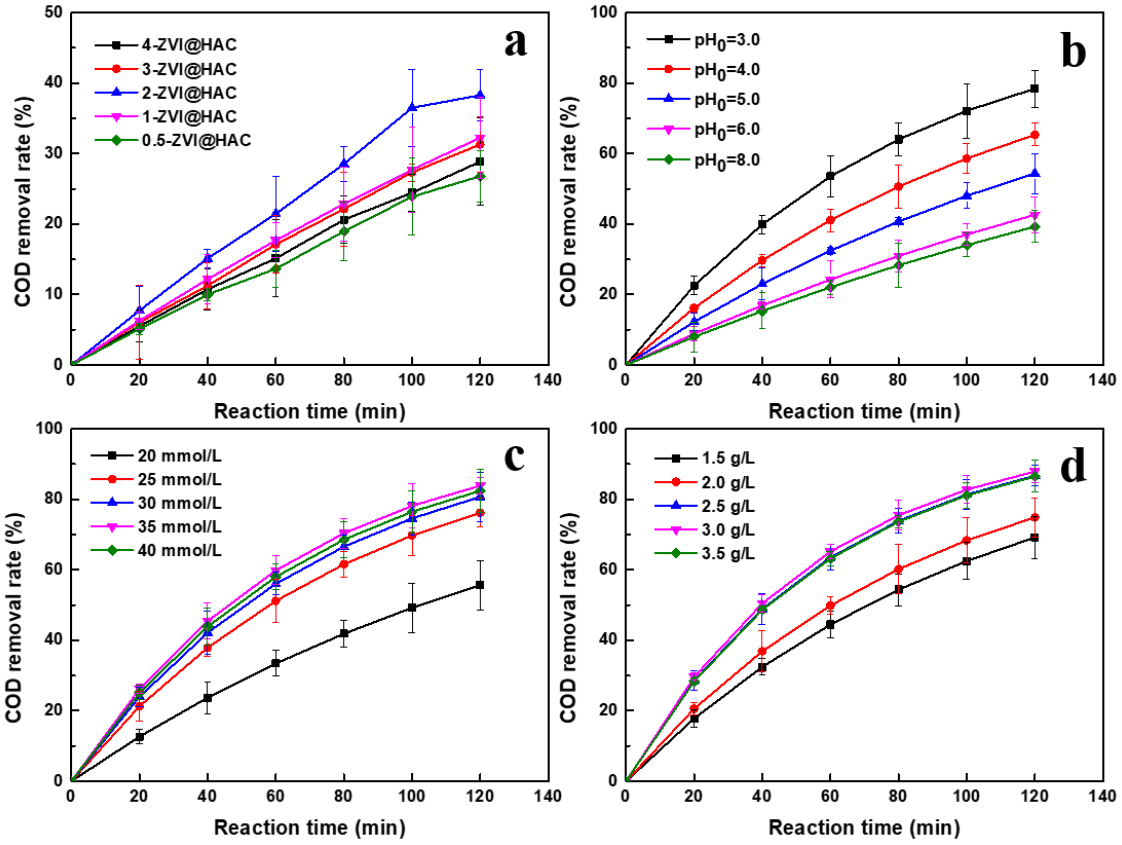

Fig. 2. Effects of iron content, pH, H_2O_2 dosage, and catalyst loading on removal of COD from pulping effluent. Conditions: (a) initial pH with no adjustment, 25 mmol/L H_2O_2, 2.5 g/L catalyst; (b) 25 mmol/L H_2O_2, 2.5 g/L catalyst; (c) pH 3.0, 2.5 g/L catalyst; and (d) pH 3.0, 35 mmol/L H_2O_2

The effect of iron content on COD removal efficiency was explored, and the results are shown in Fig. 2(a). All COD removal rates were below 40% due to the high initial pH (8.2). The activity of catalysts was relative to each other in the following order: 0.5-ZVI@HAC < 4-ZVI@HAC < 3-ZVI@HAC < 1-ZVI@HAC < 2-ZVI@HAC. This revealed that the distribution of ZVI particles on HAC had a certain effect on reactivity.

The relatively low catalytic activity of 4-ZVI@HAC was attributed to the aggregation of ZVI particles with small surface area. With the iron content decreased, ZVI particles were more evenly dispersed and the composite could have more surface area, which provided more active sites for adsorption of organic compounds and activation of H_2O_2.

The influence of initial pH on COD removal was explored at five different initial pH values. As shown in Fig. 2(b), COD removal rates increased as initial pH value decreased. When initial pH was 3.0, 78.4% of COD was removed in 120 min. This could be explained by the reaction mechanism of ZVI in Fenton-like reaction. Specifically, the first step in the oxidation of organic compounds by ZVI is the oxidation of Fe^0 by H_2O_2 under acidic conditions (Wang *et al.* 2019). Then, the produced Fe^{2+} reacts with hydrogen peroxide rapidly to generate hydroxyl radicals, which are regarded as the key oxidizing species. The formation of Fe^{2+} was boosted due to the high H^+ concentration. When initial pH was in the range of 5.0 to 8.0, the COD removal rates were below 50%. This was because of limited Fe^{2+} formation due to relatively less H^+. In addition, H_2O_2 was decomposed to oxygen and H_2O at high pH, which could reduce the generation of •OH.

The effect of H_2O_2 dosage on COD removal was investigated over a range of 15 mmol/L to 40 mmol/L. Figure 2(c) shows that COD removal rate increased from 40.6% to 80.6% in 120 min when H_2O_2 dosage was increased from 15 mmol/L to 30 mmol/L. When H_2O_2 was insufficient, the quantity of •OH was not enough to degrade organic components. As H_2O_2 dosage increased to 35 mmol/L, COD removal rate increased towards the maximum. This was because of the formation of more hydroxyl radicals. Nevertheless, when H_2O_2 dosage further increased to 40 mmol/L, COD removal rate decreased from 83.8% to 82.3%. The reason for this phenomenon was that excess H_2O_2 could be a scavenger of •OH (Eqs. 1 and 2). Compared to •OH, other radicals ($HO_2^{\bullet}$) generated from the scavenging reaction are quite unreactive toward organic compounds (Li *et al.* 2006).

$$\bullet OH + H_2O_2 \rightarrow HO_2^{\bullet} + H_2O \quad (1)$$

$$Fe^{2+} + \bullet OH + H^+ \rightarrow Fe^{3+} + H_2O \quad (2)$$

As shown in Fig. 2(d), COD removal rate increased from 69.1% to 87.8% when the catalyst loading was increased from 1.5 g/L to 3.0 g/L, which indicated that active sites were not enough when catalyst loading was lower than 3.0 g/L. When catalyst loading was increased, there were more actives sites on the surface of ZVI@HAC, which generated more •OH. However, the COD removal rate decreased slightly as catalyst loading further increased to 3.5 g/L. This might have been attributed to the scavenging reaction between •OH and Fe^{2+}.

Characterization

Figure 3 displays the SEM images of hemp fiber, HAC, and 2-ZVI@HAC. Hemp fiber has a porous and hollow pipeline structure. Large numbers of pores with different sizes were observed on the surface of HAC. Particles with a diameter between 100 nm and 500 nm were found on the surface of 2-ZVI@HAC, as shown in Fig. 3(c). Combined with the results of XRD, these particles could be ZVI particles. A certain number of ZVI particles were loaded into the pores of HAC, which was helpful for enhancing the stability of the catalyst. The EDS results showed the presence of phosphorus (Fig. S1). This could have been attributed to residual H_3PO_4. Figure 3(d) shows that the dimensions of loaded particles increased and the surface of 2-ZVI@HAC became scabrous after 4 recycles. The

reason for this phenomenon was the formation of iron oxide layers, such as Fe_3O_4, $Fe(OH)_3$, and FeOOH, covered with ZVI particles.

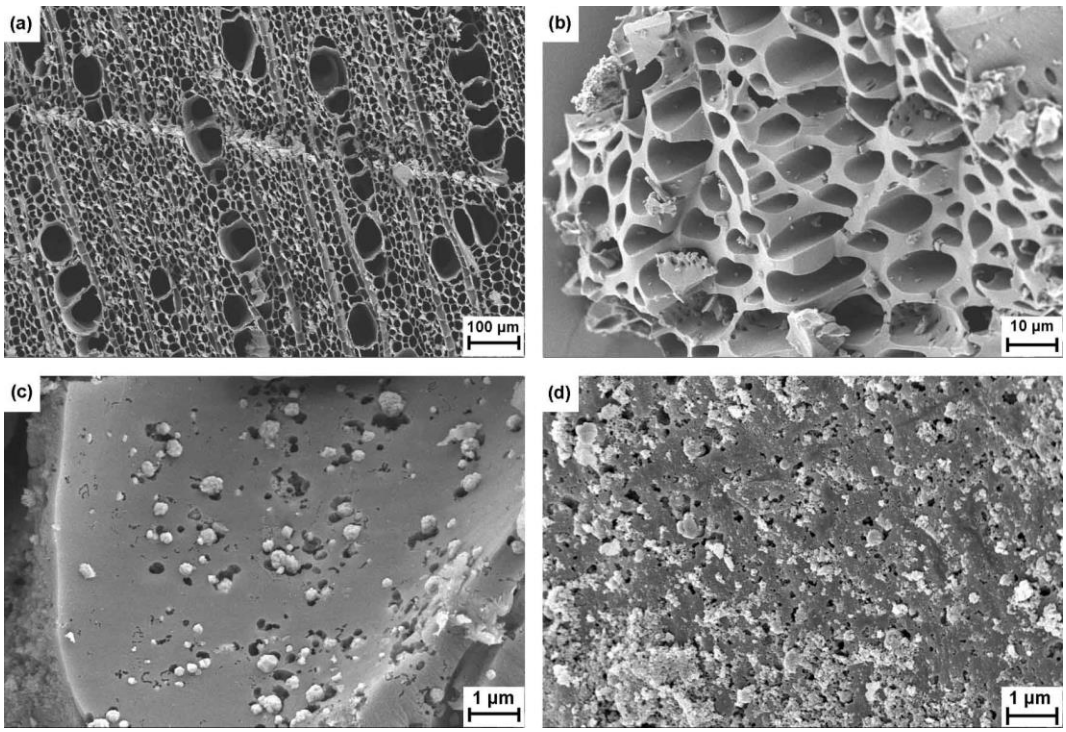

Fig. 3. SEM images of (a) hemp fiber (cross-section), (b) HAC, (c) 2-ZVI@HAC, and (d) 2-ZVI@HAC (after 4th run)

The pore properties of HAC and 2-ZVI@HAC were analyzed *via* N_2 gas sorption spectra. As shown in Fig. 4, the N_2 adsorption and desorption isotherms of both HAC and 2-ZVI@HAC were of type I.

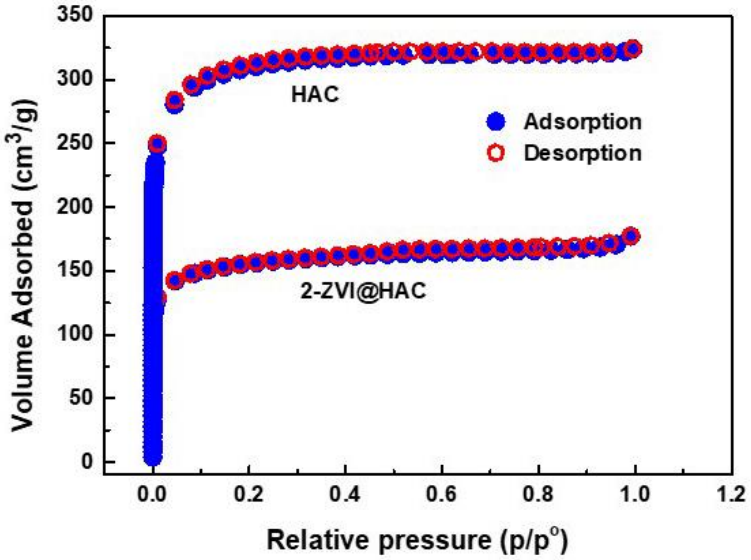

Fig. 4. N_2 adsorption/desorption isotherms onto HAC and 2-ZVI@HAC

A sharp increase in N_2 adsorption at very low relative pressure ($p/p_0 < 0.01$) was observed. This is a characteristic feature of microporous materials (Pal *et al.* 2017). The 2-ZVI@HAC generated much lower N_2 uptake, which suggested that the pore structure of HAC was inevitably destroyed by ZVI. In addition, Fig. 5 shows that the pore width of HAC was mainly between 0.8 nm and 2.0 nm. Compared with HAC, more micropores with pore widths from 0 nm to 1.0 nm were observed. This was because of the formation of new micropores in the process of calcination.

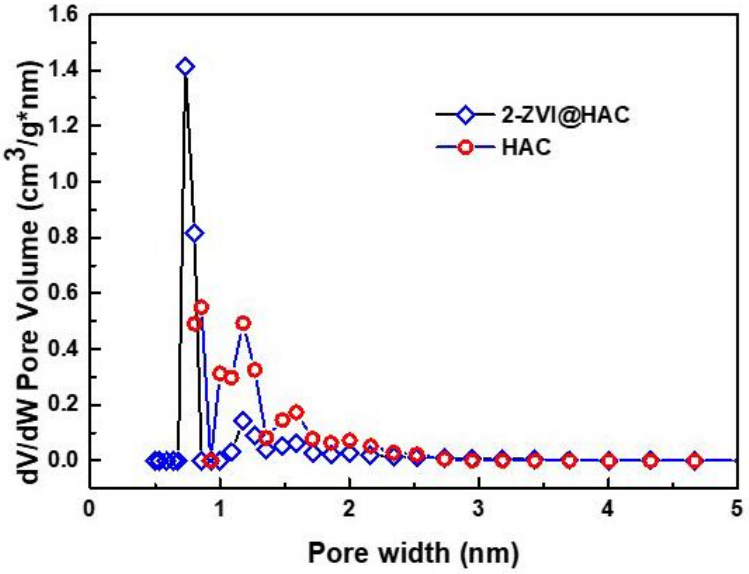

Fig. 5. Pore size distributions of HAC and 2-ZVI@HAC

Table 2. Results of BET Characterization

Samples	BET Surface Area (m^2/g)	Average Pore Diameter (nm)	Pore Volume (cm^3/g)
HAC	943.81	2.10	0.377
2-ZVI@HAC	476.32	2.20	0.187
2-ZVI@HAC (after 1st run)	691.42	2.21	0.264
2-ZVI@HAC (after 4th run)	614.15	2.60	0.205

Table 2 represents the surface properties of HAC and 2-ZVI@HAC. The BET surface area of HAC (943.81 m^2/g) was higher than several other ZVI carriers such as graphene oxide (5.33 m^2/g), biochar (194.35 m^2/g), and mesoporous carbon (686 m^2/g) (Dai *et al.* 2016; Hussain *et al.* 2017; Farooq *et al.* 2019). After loading the ZVI, the BET surface area and pore volume of catalyst were remarkably reduced. This illustrated that most pores of HAC were occupied by ZVI particles. After the fourth use, the average pore diameter of the catalyst increased noticeably, which might have been caused by waste of ZVI. Compared with the first use, the BET surface area and pore volume of the 2-ZVI@HAC slightly decreased after the fourth reuse. This indicated that the adsorption of catalyst also played a role in the Fenton-like process.

Raman spectra of HAC and 2-ZVI@HAC are shown in Fig. 6. Two predominant peaks at 1340 cm^{-1} and 1600 cm^{-1} were attributed to the defects or disordered carbon (known as the D band) and the in-plane bond stretching ordered sp^2 carbon atoms (known as the G band) (Wang *et al.* 2011). The relative intensity comparison between the I_D and

I_G was used to assess the degree of crystallinity of carbon materials (Liu and Wang 2019). Compared to HAC, a rather high I_D/I_G value (0.97) was observed for 2-ZVI@HAC, which indicated the low degree of graphitization and the high crystal defect provoked during calcination treatment. The reason for this change was substitution of HAC surface atoms by iron element. This might be the key mechanism for the increase of active sites in 2-ZVI@HAC.

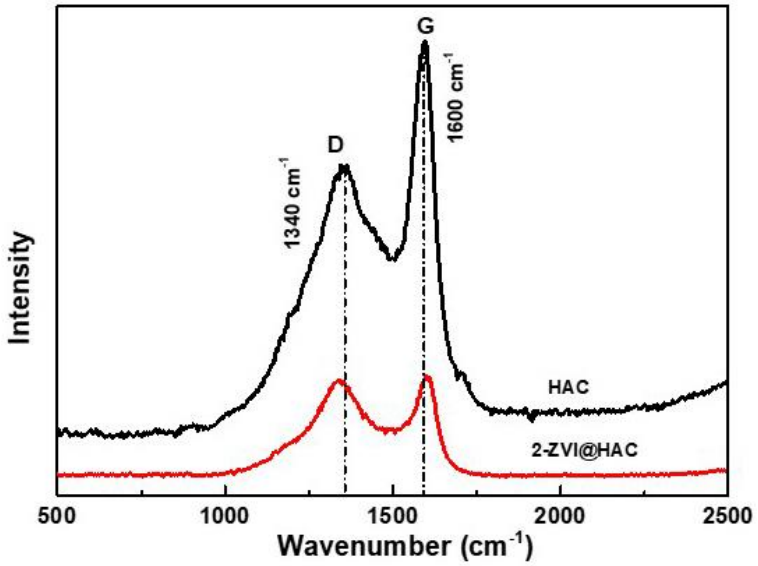

Fig. 6. Raman spectra of HAC and 2-ZVI@HAC

UV Spectroscopic Analyses and GC-MS Analyses

Organic pollutants in pulping effluent have strong adsorption in the ultraviolet spectral region (He *et al.* 2016). Thus, the degradation extent of organic pollutants can be reflected by changes in the UV-vis spectrum of the effluent before and after Fenton-like reaction. As shown in Fig. 7, UV absorbance of the effluent after reaction declined obviously.

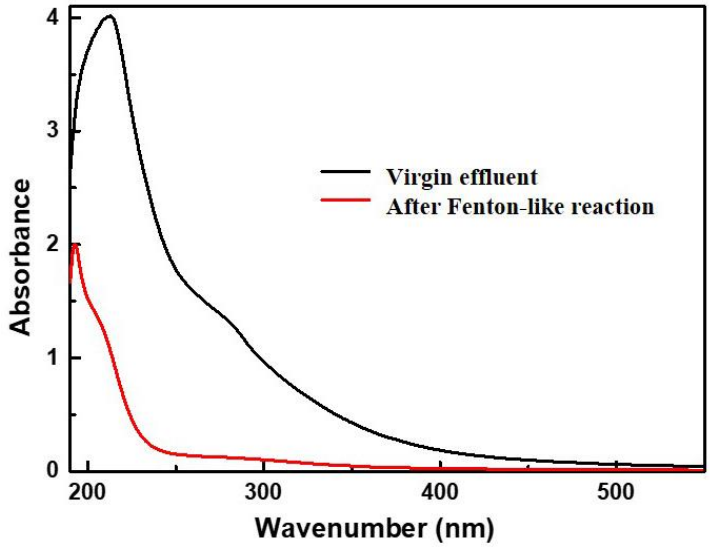

Fig. 7. UV-visible analysis of effluent

The organic compounds of effluent before and after Fenton-like oxidation were identified using GC-MS, as shown in Table S1. After Fenton-like process, the number of organic species in effluent decreased from 36 to 15. Combine the above results, organic pollutants in effluent degraded substantially after 120 min catalytic oxidation.

Reuse of ZVI@HAC

To investigate the reuse performance of 2-ZVI@HAC, spent 2-ZVI@HAC composite was collected and washed with de-ionized water, dried at 105 °C for 12 h until all water was evaporated, and then reused under the same reaction condition as described above. As shown in Fig. 8, COD removal rate remained above 58% in four runs. However, removal performance decreased gradually in the process of recycling.

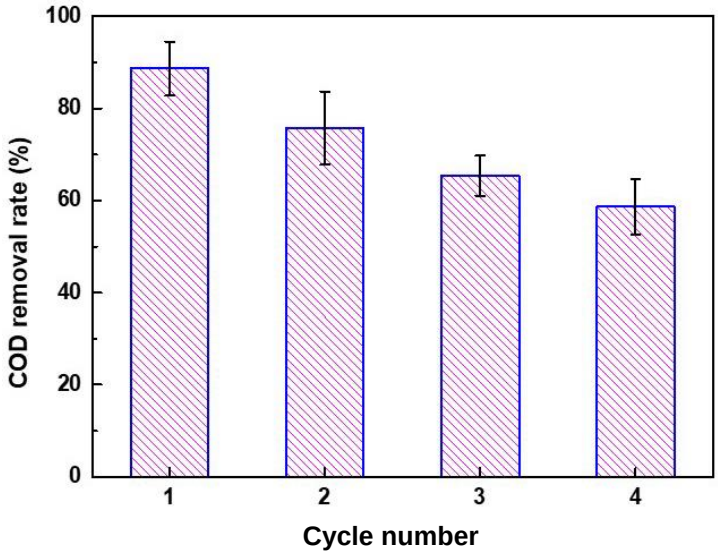

Fig. 8. Percentage of COD removal (%) using recovered 2-ZVI@HAC in four treatment cycles (initial pH = 3.0, H_2O_2 concentration = 35 mmol/L, catalyst loading = 3.0 g/L, and reaction time = 120 min)

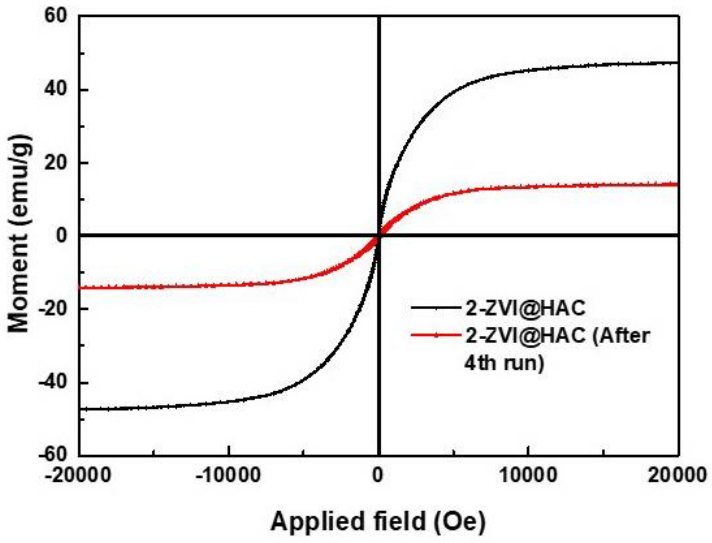

Fig. 9. Magnetic plots of 2-ZVI@HAC before runs and after the 4th run

The reduction of COD removal rate was attributed to the following: (i) decrease of surface area, (ii) wastage of ZVI particles, and (iii) reduction of adsorption capacity and catalytic surface activity *via* blocking pores by organic molecules after each use. The magnetic properties of 2-ZVI@HAC and recovered 2-ZVI@HAC (after 4th run) were investigated to test the feasibility of magnetic separation. As illustrated for VSM curves in Fig. 9, recovered 2-ZVI@HAC had a magnetic saturation (Ms) of 14.75 emu/g, which was lower than that of 2-ZVI@HAC (Ms = 47.22 emu/g). This was attributed to consumption of ZVI particles and shielding of organics on the surface of ZVI particles. As shown in Fig. S2, 2-ZVI@HAC catalyst could be recovered by applying an external magnet.

Possible Catalytic Mechanism of ZVI@HAC

Based on the above-mentioned results and discussions, a possible reaction mechanism of ZVI@HAC is proposed (Fig. 10). Herein, hydroxyl radicals are produced by the heterogeneous reaction between H_2O_2 molecules and ZVI particles. Notably, formation of •OH occurs not only in the solid phase, but also in the solution phase between H_2O_2 molecules and leached metal ions from catalyst surface. Further, the catalyst has a certain adsorption effect on organic compounds, which is conducive to accelerating the reaction between organics and •OH radicals.

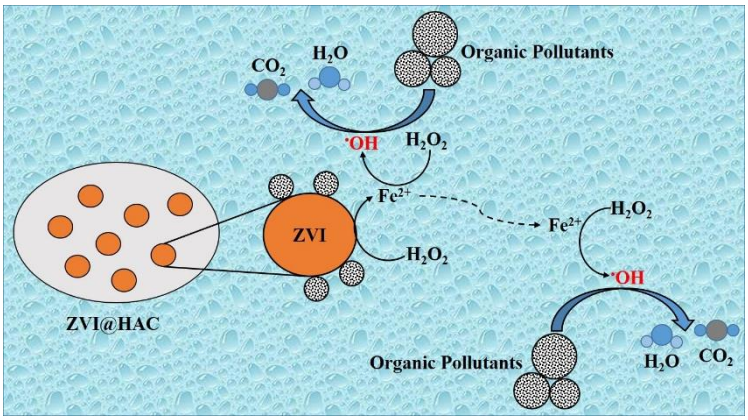

Fig. 10. Possible reaction mechanism of ZVI@HAC

CONCLUSIONS

1. The zero-valent iron / hemp activated carbon (ZVI@HAC) catalyst synthesized by immobilizing zero-valent iron particles on HAC, which had high specific surface area and porosities, proved to be an effective heterogeneous Fenton catalyst.
2. Results showed that ZVI particles were well-distributed on the surface of HAC without aggregation. Both HAC and ZVI@HAC had microporous structure. With the loading of ZVI, active sites of composites showed an increasing trend. The magnetism given by ZVI was an advantage for recycling.
3. The 2-ZVI@HAC had the best catalytic performance. The highest removal rate (87.7%) of COD was achieved at the optimal conditions (3.0 initial pH, 35 mmol/L H_2O_2, and 3.0 g/L ZVI@HAC). However, performance of the catalyst decreased gradually in the process of recycling.

4. Above all, HAC could be successfully applied as a carrier of ZVI particles. The ZVI@HAC catalyst was feasible for Fenton-like treatment of pulping effluent.

ACKNOWLEDGMENTS

The authors are grateful for the support of the Guangzhou Science & Technology Plan Projects (No. 201707020011), the Special Support Plan for High Level Talent Cultivation of Guangdong Province (No. 2014TQ01N603), the National Science and Technology Major Project (No. 2017ZX07402004), the State Key Laboratory of Pulp and Paper Engineering (No. 201831), and the Guangdong Province Science Foundation for Cultivating National Engineering Research Center for Efficient Utilization of Plant Fibers (No. 2017B090903003).

REFERENCES CITED

Arimi, M. M. (2017). "Modified natural zeolite as heterogeneous Fenton catalyst in treatment of recalcitrants in industrial effluent," *Prog. Nat. Sci.- Mater.* 27(2), 275-282. DOI: 10.1016/j.pnsc.2017.02.001

Bello, M. M., Abdul Raman, A. A., and Asghar, A. (2019). "A review on approaches for addressing the limitations of Fenton oxidation for recalcitrant wastewater treatment," *Process Saf. Environ.* 126, 119-140. DOI: 10.1016/j.psep.2019.03.028

Bhaumik, M., McCrindle, R. I., and Maity, A. (2015). "Enhanced adsorptive degradation of Congo red in aqueous solutions using polyaniline/Fe^0 composite nanofibers," *Chem. Eng. J.* 260, 716-729. DOI: 10.1016/j.cej.2014.09.014

Dai, Y., Hu, Y., Jiang, B., Zou, J., Tian, G., and Fu, H. (2016). "Carbothermal synthesis of ordered mesoporous carbon-supported nano zero-valent iron with enhanced stability and activity for hexavalent chromium reduction," *J. Hazard. Mater.* 309, 249-258. DOI: 10.1016/j.jhazmat.2015.04.013

Deng, J., Dong, H., Zhang, C., Jiang, Z., Cheng, Y., Hou, K., Zhang, L., and Fan, C. (2018). "Nanoscale zero-valent iron/biochar composite as an activator for Fenton-like removal of sulfamethazine," *Sep. Purif. Technol.* 202, 130-137. DOI: 10.1016/j.seppur.2018.03.048

Farooq, U., Danish, M., Lyu, S., Brusseau, M. L., Gu, M., Zaman, W. Q., Qiu, Z., and Sui, Q. (2019). "The impact of surface properties and dominant ions on the effectiveness of G-nZVI heterogeneous catalyst for environmental remediation," *Sci. Total Environ.* 651, 1182-1188. DOI: 10.1016/j.scitotenv.2018.09.148

He, S., Li, J., Xu, J., and Mo, L. (2016). "Enhanced removal of COD and color in paper-making wastewater by ozonation catalyzed by Fe supported on activated carbon," *BioResources* 11(4), 8396-8408. DOI: 10.15376/biores.11.4.8396-8408

He, S., Luan, P., Mo, L., Xu, J., Li, J., Zhu, L., and Zeng, J. (2018). "Mineralization of recalcitrant organic pollutants in pulp and paper mill wastewaters through ozonation catalyzed by Cu-Ce supported on Al_2O_3," *BioResources* 13(2), 3686-3703. DOI: 10.15376/biores.13.2.3686-3703

Hoch, L. B., Mack, E. J., Hydutsky, B. W., Hershman, J. M., Skluzacek, I. M., and Mallouk, T. E. (2008). "Carbothermal synthesis of carbon-supported nanoscale zero-valent iron particles for the remediation of hexavalent chromium," *Environ. Sci.*

Technol 42, 2600-2605. DOI: 10.1021/es702589u

Hussain, I., Li, M., Zhang, Y., Li, Y., Huang, S., Du, X., Liu, G., Hayat, W., and Anwar, N. (2017). "Insights into the mechanism of persulfate activation with nZVI/BC nanocomposite for the degradation of nonylphenol," *Chem. Eng. J.* 311, 163-172. DOI: 10.1016/j.cej.2016.11.085

ISO 6060. (1989). "Water quality – Determination of the chemical oxygen demand," International Organization for Standardization, Geneva, Switzerland.

Kamali, M., and Khodaparast, Z. (2015). "Review on recent developments on pulp and paper mill wastewater treatment," *Ecotox. Environ. Safe.* 114, 326-342. DOI: 10.1016/j.ecoenv.2014.05.005

Krishna, K. V., Sarkar, O., and Venkata Mohan, S. (2014). "Bioelectrochemical treatment of paper and pulp wastewater in comparison with anaerobic process: Integrating chemical coagulation with simultaneous power production," *Bioresource Technol.* 174, 142-151. DOI: 10.1016/j.biortech.2014.09.141

Kyzas, G. Z., Deliyanni, E. A., and Matis, K. A. (2016). "Activated carbons produced by pyrolysis of waste potato peels: Cobalt ions removal by adsorption," *Colloid. Surface. A* 490, 74-83. DOI: 10.1016/j.colsurfa.2015.11.038

Li, X., Elliott, D. W., and Zhang, W. (2006). "Zero-valent iron nanoparticles for abatement of environmental pollutants: Materials and engineering aspects," *Crit. Rev. Solid State Mater. Sci.* 31(4), 111-122. DOI: 10.1080/10408430601057611

Liu, S., Ge, L., Gao, S., Zhuang, L., Zhu, Z., and Wang, H. (2017). "Activated carbon derived from bio-waste hemp hurd and retted hemp hurd for CO_2 adsorption," *Compos. Commun.* 5, 27-30. DOI: 10.1016/j.coco.2017.06.002

Liu, X., and Wang, Y. (2019). "Activated carbon supported nanoscale zero-valent iron composite: Aspects of surface structure and composition," *Mater. Chem. Phys.* 222, 369-376. DOI: 10.1016/j.matchemphys.2018.10.013

Merayo, N., Hermosilla, D., Blanco, L., Cortijo, L., and Blanco, Á. (2013). "Assessing the application of advanced oxidation processes, and their combination with biological treatment, to effluents from pulp and paper industry," *J. Hazard. Mater.* 262, 420-427. DOI: 10.1016/j.jhazmat.2013.09.005

Mortazavian, S., An, H., Chun, D., and Moon, J. (2018). "Activated carbon impregnated by zero-valent iron nanoparticles (AC/nZVI) optimized for simultaneous adsorption and reduction of aqueous hexavalent chromium: Material characterizations and kinetic studies," *Chem. Eng. J.* 353, 781-795. DOI: 10.1016/j.cej.2018.07.170

Nabais, J. M. V., Nunes, P., Carrott, P. J. M., Ribeiro Carrott, M. M. L., García, A. M., and Díaz-Díez, M. A. (2008). "Production of activated carbons from coffee endocarp by CO_2 and steam activation," *Fuel Process. Technol.* 89(3), 262-268. DOI: 10.1016/j.fuproc.2007.11.030

Neyens, E., and Baeyens, J., (2003). "A review of classic Fenton's peroxidation as an advanced oxidation technique," *J. Hazard. Mater.* 98 (1-3), 33-50. DOI: 10.1016/S0304-3894(02)00282-0

Pal, A., Thu, K., Mitra, S., El-Sharkawy, I. I., Saha, B. B., Kil, H.-S., Yoon, S.-H., and Miyawaki, J. (2017). "Study on biomass derived activated carbons for adsorptive heat pump application," *Int. J. Heat Mass Tran.* 110, 7-19. DOI: 10.1016/j.ijheatmasstransfer.2017.02.081

Rosas, J., Bedia, J., Rodríguez-Mirasol, J., and Cordero, T. (2008). "Preparation of hemp-derived activated carbon monoliths. Adsorption of water vapor," *Ind. Eng. Chem. Res.* 47(4), 1288-1296. DOI: 10.1021/ie070924w

Rubeena, K. K., Hari Prasad Reddy, P., Laiju, A. R., and Nidheesh, P. V. (2018). "Iron impregnated biochars as heterogeneous Fenton catalyst for the degradation of acid red 1 dye," *J. Environ. Manage.* 226, 320-328. DOI: 10.1016/j.jenvman.2018.08.055

Su, C., Li, Y., He, Y., Liu, L., Wang, X., and Liu, L. (2015). "Al_2O_3-doped for enhancing ethanol sensing properties of α-Fe_2O_3 nanotubes," *Mater. Sci. Semicon. Proc.* 39, 49-53. DOI: 10.1016/j.mssp.2015.04.043

Tosco, T., Petrangeli Papini, M., Cruz Viggi, C., and Sethi, R. (2014). "Nanoscale zerovalent iron particles for groundwater remediation: A review," *J. Clean. Prod.* 77, 10-21. DOI: 10.1016/j.jclepro.2013.12.026

Vandarkuzhali, S. A. A., Karthikeyan, S., Viswanathan, B., and Pachamuthu, M. P. (2018). "*Arachis hypogaea* derived activated carbon/Pt catalyst: Reduction of organic dyes," *Surf. Interfaces* 13, 101-111. DOI: 10.1016/j.surfin.2018.07.005

Veerakumar, P., Panneer Muthuselvam, I., Hung, C.-T., Lin, K.-C., Chou, F.-C., and Liu, S.-B. (2016). "Biomass-derived activated carbon supported Fe_3O_4 nanoparticles as recyclable catalysts for reduction of nitroarenes," *ACS Sustain. Chem. Eng.* 4(12), 6772-6782. DOI: 10.1021/acssuschemeng.6b01727

Vukčević, M. M., Kalijadis, A. M., Vasiljević, T. M., Babić, B. M., Laušević, Z. V, and Laušević, M. D. (2015). "Production of activated carbon derived from waste hemp (*Cannabis sativa*) fibers and its performance in pesticide adsorption," *Micropor. Mesopor. Mat.* 214, 156-165. DOI: 10.1016/j.micromeso.2015.05.012

Vukčević, M., Pejić, B., Kalijadis, A., Pajić-Lijaković, I., Kostić, M., Laušević, Z., and Laušević, M. (2014). "Carbon materials from waste short hemp fibers as a sorbent for heavy metal ions – Mathematical modeling of sorbent structure and ions transport," *Chem. Eng. J.* 235, 284-292. DOI: 10.1016/j.cej.2013.09.047

Wang, J.-Z., Zhong, C., Wexler, D., Idris, N. H., Wang, Z.-X., Chen, L.-Q., and Liu, H.-K. (2011). "Graphene-encapsulated Fe_3O_4 nanoparticles with 3D laminated structure as superior anode in lithium ion batteries," *Chemistry – A European Journal* 17(2), 661-667. DOI: 10.1002/chem.201001348

Wang, Z., Li, J., Tan, W., Wu, X., Lin, H., and Zhang, H. (2019). "Removal of COD from landfill leachate by advanced Fenton process combined with electrolysis," *Sep. Purif. Technol.* 208, 3-11. DOI: 10.1016/j.seppur.2018.06.048

Yang, K., Peng, J., Srinivasakannan, C., Zhang, L., Xia, H., and Duan, X. (2010). "Preparation of high surface area activated carbon from coconut shells using microwave heating," *Bioresource Technol.* 101(15), 6163-6169. DOI: 10.1016/j.biortech.2010.03.001

Yiu, H. H. P., McBain, S. C., Lethbridge, Z. A. D., Lees, M. R., and Dobson, J. (2010). "Preparation and characterization of polyethylenimine-coated Fe_3O_4-MCM-48 nanocomposite particles as a novel agent for magnet-assisted transfection," *J. Biomed. Mater. Res. A* 92A(1), 386-392. DOI: 10.1002/jbm.a.32363

Zhang, W., Qian, L., Ouyang, D., Chen, Y., Han, L., and Chen, M. (2019). "Effective removal of Cr(VI) by attapulgite-supported nanoscale zero-valent iron from aqueous solution: Enhanced adsorption and crystallization," *Chemosphere* 221, 683-692. DOI: 10.1016/j.chemosphere.2019.01.070

Article submitted: November 21, 2019; Peer review completed: Jan. 24, 2020; Revised version received and accepted: May 7, 2020; Published: May 13, 2020.
DOI: 10.15376/biores.15.3.4996-5011

APPENDIX

Supplementary Information

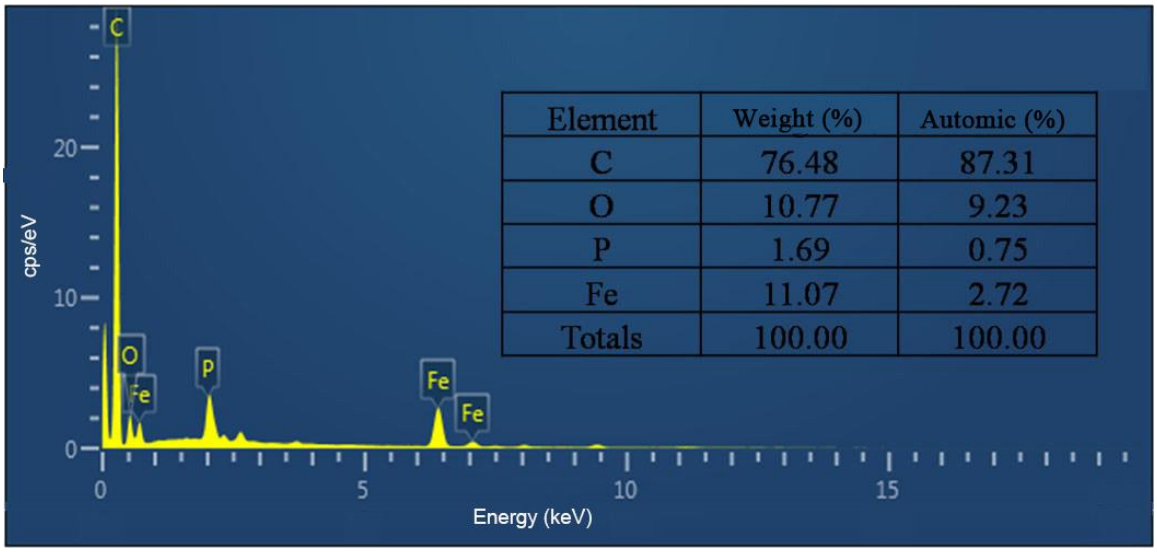

Element	Weight (%)	Automic (%)
C	76.48	87.31
O	10.77	9.23
P	1.69	0.75
Fe	11.07	2.72
Totals	100.00	100.00

Fig. S1. EDS spectrum of 2-ZVI@HAC

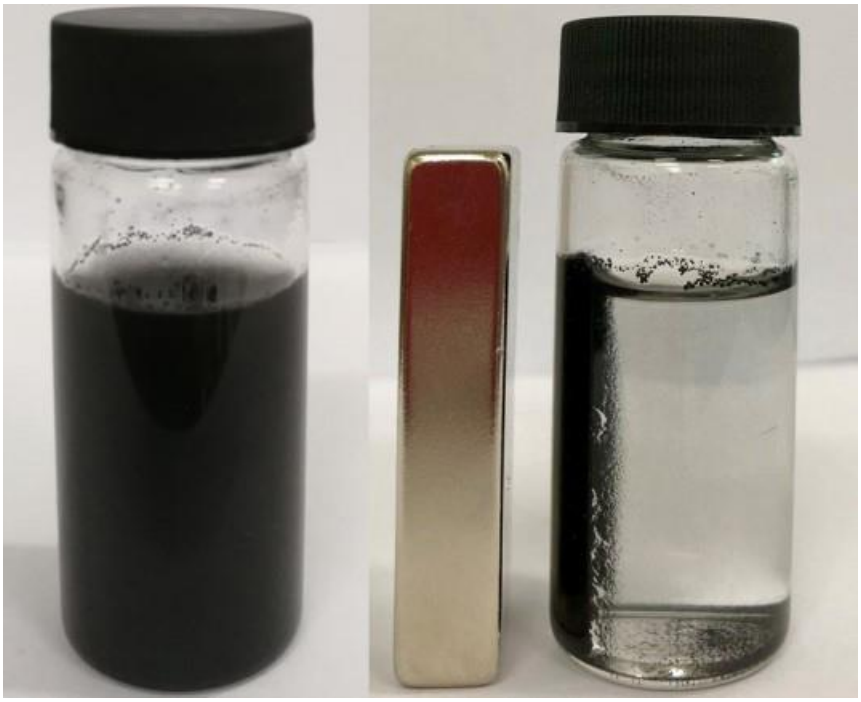

Fig. S2. Attraction of catalyst by an external magnetic field

Table S1. Organic Compounds of the Effluent Detected by GC-MS

Number	ID	Area/%	
		Virgin effluent	After oxidation
1	Styrene	2.01	1.99
2	Heptane, 2,2,4,6,6-pentamethyl-	0.34	11.01
3	Octane, 5-ethyl-2-methyl-	0.73	0.00
4	Nonanal	2.02	0.00
5	Benzene, 1-methyl-2-nitro-	2.32	0.00
6	Dodecane	0.84	1.15
7	Carbonic acid, hexadecyl prop-1-en -2-yl ester	0.37	0.00
8	Octane, 5-ethyl-2-methyl-	0.88	0.00
9	Dodecane, 2,6,11-trimethyl-	0.56	0.00
10	Phenol, 2-methoxy-4-propyl-	0.72	0.00
11	Anthracene, 9-ethyl-9,10-dihydro-	0.56	0.00
12	Naphthalene, 1-bromo-	3.40	0.00
13	Dotriacontane, 1-iodo-	0.73	0.00
14	3-Pentadecanone	0.54	2.94
15	Cyclopentane, undecyl-	1.15	0.00
16	3-Heptadecanone	0.50	1.37
17	Dibutyl phthalate	0.58	0.00
18	1-Nonadecene	1.19	3.21
19	Ethyl pentafluoropropionate	1.28	0.00
20	9-Tricosene, (Z)-	5.42	1.70
21	1-Heptacosanol	1.08	0.00
22	Nonadecyl pentafluoropropionate	0.63	0.00
23	Decahydro-8a-ethyl-1,1,4a,6-tetram ethylnaphthalene	0.67	0.00
24	Erucic acid	0.42	0.00
25	Pentadec-7-ene, 7-bromomethyl-	0.80	0.00
27	Phenol, 2,2'-methylenebis[6-(1,1-d imethylethyl)-4-methyl-	3.67	38.15
28	17-Pentatriacontene	1.21	0.00
29	Dotriacontyl pentafluoropropionate	0.55	0.00
30	Di-n-octyl phthalate	2.90	0.00
31	Z-12-Pentacosene	0.26	0.00
32	Tetracosane	2.34	1.70
33	11,13-Dimethyl-12-tetradecen-1-ol acetate	1.72	2.96
34	1-Hexacosene	1.48	0.00
35	Tetrapentacontane, 1,54-dibromo-	1.77	0.00
36	9-Octadecenamide, (Z)-	54.33	22.87
37	Toluene	0.00	4.91
38	Hexane, 2,5-dimethyl-	0.00	1.81
39	Undecane, 4,7-dimethyl-	0.00	1.49
40	Octadecane, 1-iodo-	0.00	1.37
41	1-Docosene	0.00	1.36